Reduced ^{64}Cu Uptake and Tumor Growth Inhibition by Knockdown of Human Copper Transporter 1 in Xenograft Mouse Model of Prostate Cancer

Huawei Cai[1], Jiu-sheng Wu[2], Otto Muzik[2], Jer-Tsong Hsieh[3,4], Robert J. Lee[5], and Fangyu Peng[1,4,6]

[1]Department of Radiology, University of Texas Southwestern Medical Center, Dallas, Texas; [2]Carman and Ann Adams Department of Pediatrics, School of Medicine, Wayne State University, Detroit, Michigan; [3]Department of Urology, University of Texas Southwestern Medical Center, Dallas, Texas; [4]Harold C. Simmons Comprehensive Cancer Center, University of Texas Southwestern Medical Center, Dallas, Texas; [5]College of Pharmacy, Ohio State University, Columbus, Ohio; and [6]Advanced Imaging Research Center, University of Texas Southwestern Medical Center, Dallas, Texas

Copper is an element required for cell proliferation and angiogenesis. Human prostate cancer xenografts with increased ^{64}Cu radioactivity were visualized previously by PET using ^{64}CuCl$_2$ as a radiotracer (^{64}CuCl$_2$ PET). This study aimed to determine whether the increased tumor ^{64}Cu radioactivity was due to increased cellular uptake of ^{64}Cu mediated by human copper transporter 1 (hCtr1) or simply due to nonspecific binding of ionic ^{64}CuCl$_2$ to tumor tissue. In addition, the functional role of hCtr1 in proliferation of prostate cancer cells and tumor growth was also assessed. **Methods:** A lentiviral vector encoding short-hairpin RNA specific for hCtr1 (Lenti-hCtr1-shRNA) was constructed for RNA interference–mediated knockdown of hCtr1 expression in prostate cancer cells. The degree of hCtr1 knockdown was determined by Western blot, and the effect of hCtr1 knockdown on copper uptake and proliferation were examined in vitro by cellular ^{64}Cu uptake and cell proliferation assays. The effects of hCtr1 knockdown on tumor uptake of ^{64}Cu were determined by PET quantification and tissue radioactivity assay. The effects of hCtr1 knockdown on tumor growth were assessed by PET/CT and tumor size measurement with a caliper. **Results:** RNA interference–mediated knockdown of hCtr1 was associated with the reduced cellular uptake of ^{64}Cu and the suppression of prostate cancer cell proliferation in vitro. At 24 h after intravenous injection of the tracer ^{64}CuCl$_2$, the ^{64}Cu uptake by the tumors with knockdown of hCtr1 (4.02 ± 0.31 percentage injected dose per gram [%ID/g] in Lenti-hCtr1-shRNA-PC-3 and 2.30 ± 0.59 %ID/g in Lenti-hCtr1-shRNA-DU-145) was significantly lower than the ^{64}Cu uptake by the control tumors without knockdown of hCtr1 (7.21 ± 1.48 %ID/g in Lenti-SCR-shRNA-PC-3 and 5.57 ± 1.20 %ID/g in Lenti-SCR-shRNA-DU-145, $P < 0.001$) by PET quantification. Moreover, the volumes of prostate cancer xenograft tumors with knockdown of hCtr1 (179 ± 111 mm^3 for Lenti-hCtr1-shRNA-PC-3 or 39 ± 22 mm^3 for Lenti-hCtr1-shRNA-DU-145) were significantly smaller than those without knockdown of hCtr1 (536 ± 191 mm^3 for Lenti- SCR-shRNA-PC-3 or 208 ± 104 mm^3 for Lenti-SCR-shRNA-DU-145, $P < 0.01$). **Conclusion:** Overall, data indicated that hCtr1 is a promising theranostic target, which can be further developed for metabolic imaging of prostate cancer using ^{64}CuCl$_2$ PET/CT and personalized cancer therapy targeting copper metabolism.

Prostate cancer is a complex, genetically heterogeneous disease with variable clinical manifestations (1,2). PET is useful for the noninvasive assessment of metabolic activities of prostate cancer and monitoring response to treatment (3). Multiple radiopharmaceuticals were developed for PET of various metabolic pathways in prostate cancer, such as metabolism of glucose, lipid, and choline and synthesis of DNA and protein molecules. These radiotracers include ^{18}F-FDG (4), ^{11}C-choline (5), ^{18}F-choline (6), ^{18}F-fluoroethylcholine (7), ^{11}C-acetate (8), ^{18}F-FMAU (FMAU is 1-(2′-deoxy-2′-fluoro-β-D-arabinofuranosyl)thymine) (9), and ^{11}C-methionine (10). Given the genetic and metabolic heterogeneity of prostate cancer, there is need for additional radiotracers for PET imaging of other metabolic pathways in prostate cancer.

Copper is known to be critical for cell proliferation, angiogenesis, and tumor growth (11–13), and increased copper ions were detected in cancer tissues (14,15). Exploring copper metabolism as an imaging biomarker, we demonstrated that human prostate cancer xenografts with increased ^{64}Cu radioactivity could be visualized by PET using ^{64}CuCl$_2$ as a tracer (16). The expression of human copper transporter 1 (hCtr1), a high-affinity influx copper transporter (17), was demonstrated in prostate cancer xenograft tissues by immunohistochemistry analysis (16). Using RNA interference (RNAi) technology (18), this study aimed to determine whether increased ^{64}Cu radioactivity in prostate cancer xenografts visualized by PET was caused by increased cellular uptake of ^{64}Cu mediated by influx copper transporter activity of hCtr1. The effect of hCtr1 knockdown on cell proliferation was examined in vitro, and the effect of hCtr1 knockdown on tumor growth was examined in vivo by comparing the size of the tumors with knockdown of hCtr1 with the size of the tumors without knockdown of hCtr1. Overall, data support hCtr1 as a new biomarker for metabolic imaging of human prostate cancer using ^{64}CuCl$_2$ PET/CT and as a promising target for prostate cancer therapy targeting copper metabolism.

MATERIALS AND METHODS

Cells, Reagents, and Radiopharmaceuticals

The human prostate cancer cell line PC-3 (androgen receptor–negative) and C4-2 (androgen receptor–positive), a subline of LNCaP cells (American Type Culture Collection [ATCC]), were cultured in T-medium (Life Technologies) supplemented with 5% fetal bovine serum (FBS) and antibiotics (penicillin [100 U/mL] and streptomycin [100 mg/mL]) from Biosource International. The human prostate cancer cell line Du-145 (androgen receptor–negative), purchased from ATCC, was cultured in RPMI1640 medium supplemented with 10% FBS and antibiotics. Normal prostate epithelia cells (Lonza) and immortalized prostate epithelial cells (RWPE-1, RWPE-2, and PZ-HPV-7), purchased from ATCC, were cultured in prostate epithelial cell growth medium (PrEGM) supplemented with growth factors, cytokines, and supplements supplied in the SingleQuots kit (Lonza), 10% FBS, and antibiotics. Recombinant hCtr1 protein (19) was a gift from Vinzenz M. Unger at Yale University. Polyclonal antibody specific for hCtr1 was prepared using a recombinant hCtr1 protein derived from the first 67 amino acid residues at the N terminus of hCtr1 (17,20), as described in the supplemental material (available at http://jnm.snmjournals.org). The ^{64}Cu radionuclide (half-life, 12.7 h; decay characteristics β^{+}, 19%, and β^{-}, 40%) was produced in a cyclotron with a radionuclide purity greater than 99% and was supplied as ^{64}CuCl$_2$ in an HCl solution (0.1 mol/L) by the Mallinckrodt Institute of Radiology, Washington University.

Construction of hCtr1 Short Hairpin RNA (shRNA) Lentiviral Vector

A lentiviral vector encoding hCtr1 shRNA (Lenti-hCtr1-shRNA virus) was constructed as described previously (21,22). Briefly, 4 plasmid vectors encoding shRNA specific for hCtr1 and 1 plasmid encoding nonspecific, scrambled shRNA were constructed as described in the supplemental material. The hCtr1 shRNA sequence (GGAGTACACTTTCATGTGATT) was polymerase chain reaction (PCR)–amplified from the hCtr1 shRNA plasmid vector 2 and inserted into the BamHI and EcoRI site of a pGreenPurolenti-shRNA expression vector (System Biosciences). This lentiviral vector contains a puromycin-resistance gene to enable drug selection of target cells stably expressing the siRNA after transduction of the cells with lentivirus-encoding shRNA. At 72 h after transfection of 293 cells with a mixture of pLenti-hCtr1-shRNA and lentiviral packaging plasmid DNA, the supernatants containing lentivirus particles were harvested and the titers (pfu/mL) of Lenti-hCtr1-shRNA virus were determined, using an Ultra Rapid lentiviral titer kit (System Biosciences). Stock solution of the Lenti-hCtr1-shRNA virus was stored at −80°C for use within 6 months after preparation. A negative control lentiviral vector (Lenti-SCR-shRNA virus) encoding scrambled (SCR) shRNA sequence (Supplemental Table 1) was also prepared using the same method as described above. The expression of hCtr1 in the cells transduced by the lentivirus was examined by Western blot in a method as described in the supplemental material.

Cell ^{64}Cu Uptake and Proliferation Assays

To assess cellular copper uptake mediated by hCtr1, the cells were seeded into a 24-well plate (5×10^4 cells/well) and cultured in medium without serum under a serum starvation condition for 24 h. After incubation of the cells with ^{64}CuCl$_2$ (74 kBq or 2 μCi/well) at 37°C for 1 h, the cells were harvested and washed 3 times with cold phosphate-buffered saline. The radioactivity of the cells was counted with a Packard Cobra II Gamma Counter (Perkin-Elmer). A cell proliferation assay was conducted using a CCK-8 Cell Proliferation Assay kit (Dojindo) as described in the supplemental material, based on the method described previously (23). The experiment was conducted in triplicate for each point and repeated 3 times.

Small-Animal PET/CT

All animal experiments were conducted under the protocol approved by the University of Texas Southwestern Institutional Animal Care and Use Committee. PET of athymic *nu/nu* mice (male; age, 4–5 wks) bearing human prostate cancer xenografts was performed using a Siemens Inveon PET/CT Multimodality System as described previously (16,24). Briefly, a structural CT scan of tumor-bearing mice was acquired (80 kV, 500 μA) with a pixel size of approximately 0.1 mm to create an anatomic image that was subsequently used for attenuation correction of the PET emission data. After conclusion of the CT scan, mice were injected with the tracer ^{64}CuCl$_2$ (74 kBq or 2 μCi/g of body weight) intravenously via the tail vein. Static whole-body imaging was performed at 2 and 24 h after intravenous injection of the tracer, which consisted of 2 overlapping frames of 15 min for each frame. On completion of the PET/CT at 24 h after injection, a tissue radioactivity assay was performed, and tissue radioactivity was calculated and expressed as decay-corrected percentage injected dose per gram of tissue (%ID/g) as described previously (16). The size of the postmortem tumors was measured with a caliper, and tumor volumes were calculated using an ellipsoidal formula ($1/2 \times (\text{length} \times \text{width}^2)$) modified from that described previously (25).

PET Quantitative Analysis

PET images were reconstructed using the ordered-subsets expectation maximization 3-dimensional algorithm and analyzed using the Inveon Research Workplace (IRW) software (Siemens), which allows fusion of CT and PET image volumes, the reslicing of fused images into arbitrary views, and the definition of regions of interest. Static whole-body images obtained at 2 and 24 h were converted to decay-corrected images representing the %ID/g by normalizing the activity concentration in each pixel (MBq/cm^3) by the injected activity (MBq) and multiplying the result by 100%. Moreover, we used the conversion 1 cm^3 = 1 g.

Statistical Analysis

Independent sample *t* tests were applied to assess significant differences in cellular ^{64}Cu uptake and cell proliferation in vitro between the cells with or without knockdown of hCtr1. Moreover, paired *t* tests were applied to assess significant differences in tumor ^{64}Cu uptake (ID%/g) and volume between prostate cancer xenografts with or without knockdown of hCtr1. A *P* value of less than 0.05 was considered to represent statistical significance.

RESULTS

Expression of hCtr1 in Prostate Cancer Cells

Polyclonal antibodies specific for hCtr1 were obtained by immunization of rabbits with recombinant hCtr1 protein encompassing the first 67 amino acid residues of extracellular domain of hCtr1 and affinity chromatography purification of hCtr1 antibodies from rabbit antiserum (Fig. 1A). The expression of hCtr1 in prostate cancer [Fig. 1] cells (PC-3, Du-145, and C4-2), immortalized prostate epithelial cells containing HPV oncogene (RWPE-1, RWPE-2, and PZ-HPV-7), and normal prostate epithelial cells was detected by Western blot using polyclonal antibodies specific for hCtr1 (Fig. 1B). Densitometry semiquantitative analysis of Western blot demonstrated elevated expression of hCtr1 in prostate cancer cells (327% higher in PC-3, 425% higher in DU-145, 408% higher in C4-2) and immortalized prostate epithelial cells (279% higher in PZ-HPV-7, 386% higher in RWPE-1, and 349% higher in RWPE-2), compared with expression of hCtr1 (set as 100%) in normal prostate epithelial cells.

Reduction of Copper Uptake and Suppression of Cell Proliferation by Knockdown of hCtr1

Four plasmid vectors encoding shRNA sequence targeting different regions of the hCtr1 gene were constructed for knockdown
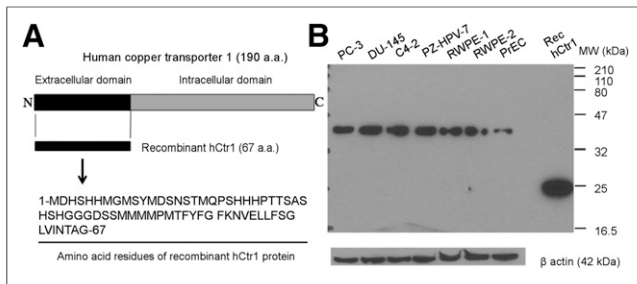
FIGURE 1. Expression of hCtr1 in prostate cancer cells by Western Blot. (A) Schematic presentation of amino acid sequence of recombinant hCtr1 protein used for preparation of polyclonal antibody specific for hCtr1. (B) Western blot of hCtr1 in prostate cancer cells (lane 1, PC-3; lane 2, DU-145; lane 3, C4-2), immortalized prostate epithelial cells containing HPV oncogene (lane 4, PZ-HPV-7; lane 5, RWPE-1; lane 6, RWPE-2), and normal prostate epithelial cells (lane 7). Loading amount was 60 μg of total cellular protein/lane for lanes 1–7. Rec hCtr1 = recombinant hCtr1 protein (30 ng/lane).

[Fig. 2] of hCtr1 expression in prostate cancer cells. As shown in Figure 2A, the #2 hCtr1 shRNA plasmid showed highest efficacy for knocking down the endogenous hCtr1 in prostate cancer cells, among 4 different hCtr1 shRNA plasmid vectors tested. hCtr1 messenger RNA (mRNA) level in the puromycin-resistant PC-3 cells transfected with the #2 hCtr1 shRNA plasmid was determined to be 22% of hCtr1 mRNA detected in the puromycin-resistant PC-3 cells transfected with SCR-shRNA plasmid or PC-3 cells without plasmid transfection by a real-time quantitative reverse transcription-PCR assay (qRT-PCR). The level of hCtr1 mRNA detected in the puromycin-resistant PC-3 cells transfected with #2 hCtr1 shRNA plasmid was determined to be 22% of the hCtr1 mRNA level detected in the puromycin-resistant PC-3 cells transfected with SCR-shRNA plasmid or PC-3 cells without plasmid transfection by qRT-PCR. Meanwhile, the levels of hCtr1 mRNA level detected
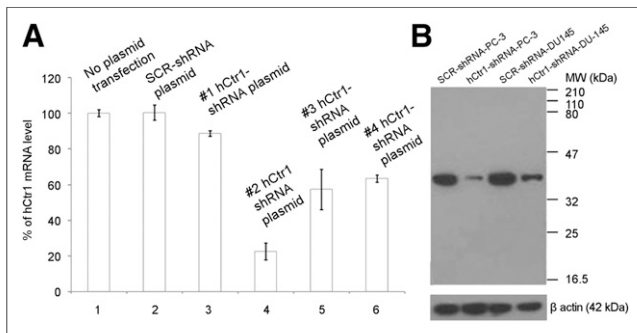
in the puromycin-resistant PC-3 cells transfected with the other 3 hCtr1 shRNA plasmids (#1, #3, and #4 hCtr1 shRNA plasmids) were determined to be 89%, 57%, and 63% of the hCtr1 mRNA level detected in the puromycin-resistant PC-3 cells transfected with SCR-shRNA plasmid or PC-3 cells without plasmid transfection by qRT-PCR, respectively. A Lenti-viral vector containing hCtr1 shRNA sequence (GGAGTACACTTTCATGTGATT) derived from #2 hCtr1 shRNA plasmid, Lenti-hCtr1-shRNA virus, was constructed and used for constant knockdown of hCtr1 in prostate cancer cells. A Lenti-viral vector encoding scrambled shRNA sequence, Lenti-SCR-shRNA virus, was constructed and used as a control. The expression of hCtr1 in the puromycin-resistant PC-3 cells transduced with Lenti-hCtr1-shRNA virus (Lenti-hCtr1-shRNA-PC-3 cells) was knockdown to 20% of hCtr1 expression in the puromycin-resistant PC-3 cells transduced with Lenti-SCR-shRNA virus (Lenti-SCR-shRNA-PC-3 cells) by Western blot (Fig. 2B). Similarly, the expression of hCtr1 in the puromycin-resistant DU-145 cells transduced with Lenti-hCtr1-shRNA virus (Lenti-hCtr1-shRNA-DU145 cells) was knockdown to 25% of hCtr1 expression in the puromycin-resistant DU-145 cells transduced with Lenti-SCR-shRNA virus (Lenti-SCR-shRNA-DU145 cells, Fig. 2B). Knockdown of hCtr1 resulted in the reduction of copper uptake by these cells (Fig. 3). [Fig. 3] After incubation with $^{64}CuCl_2$ (74 kBq or 2 μCi/well) for 24 h, ^{64}Cu radioactivity of the Lenti-hCtr1-shRNA-PC-3 cells (154 ± 7 cpm/10^4 cells) or Lenti-hCtr1-shRNA-DU-145 cells (108 ± 17 cpm/10^4 cells) was lower than ^{64}Cu radioactivity of the control Lenti-SCR-shRNA-PC-3 cells (585 ± 52 cpm/10^4 cells, $P = 0.04$) or Lenti-SCR-shRNA-DU-145 cells (481 ± 23 cpm/10^4 cells, $P < 0.01$). Furthermore, knockdown of hCtr1 resulted in slower proliferation of PC-3 and DU-145 cells (Fig. 4). At the end of the 72-h culture, [Fig. 4] there was a significant difference between the proliferation of the cells with knockdown of hCtr1 (458% ± 64% of inoculated cells for Lenti-hCtr1-shRNA-PC-3 cells and 804% ± 39% of inoculated

FIGURE 2. Knockdown of hCtr1 in prostate cancer cells by qRT-PCR and Western blot. (A) Quantity of hCtr1 mRNA in puromycin-resistant PC-3 cells transfected with plasmid encoding hCtr1 shRNA was determined by qRT-PCR and compared with hCtr1 mRNA in wild-type PC-3 cells without plasmid transfection and puromycin-resistant PC-3 cells transfected with SCR-shRNA plasmid. Among 4 hCtr1-shRNA plasmids, #2 hCtr1-shRNA plasmid showed highest efficacy for knocking down hCtr1 in PC-3 cells. (B) Knockdown of hCtr1 in puromycin-resistant PC-3 and DU-145 prostate cancer cells transduced with Lenti-hCtr1-shRNA virus encoding hCtr1 shRNA sequence derived from #2 hCtr1-shRNA plasmid by Western blot. SCR-shRNA PC-3, control Lenti-SCR-shRNA PC-3 cells; hCtr1-shRNA PC-3, Lenti-hCtr1-shRNA PC-3 cells; SCR-shRNA DU-145, control Lenti-SCR-shRNA DU-145 cells; hCtr1-shRNA DU-145, Lenti-hCtr1-shRNA DU-145 cells. Loading amount for lanes 1–4 = 60 μg/lane. Error bar, SD.
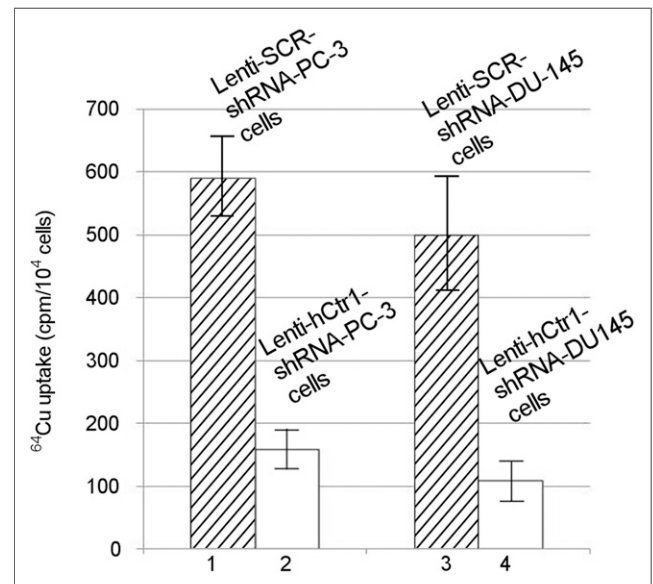

FIGURE 3. Reduced cellular copper uptake by prostate cancer cells after knocking down hCtr1 expression. ^{64}Cu radioactivity of cells with knockdown of hCtr1 (Lenti-hCtr1-shRNA-PC-3 cells and Lenti-hCtr1-shRNA-DU145 cells) was significantly lower than that of cells without knockdown of hCtr1 (Lenti-SCR-shRNA-PC-3 cells and Lenti-SCR-shRNA-DU-145 cells), at 1 h after incubation with $^{64}CuCl_2$. Error bar, SD.
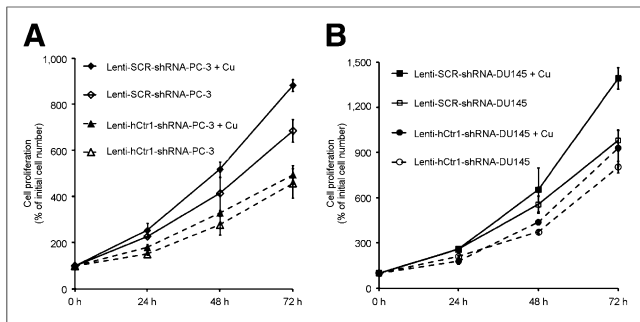
FIGURE 4. Effects of hCtr1 knockdown on prostate cancer cell proliferation in vitro. (A) Proliferation of PC-3 cells with knockdown of hCtr1 (Lenti-hCtr1-shRNA-PC-3 cells) was significantly slower than proliferation of cells without knockdown of hCtr1 (Lenti-SCR-shRNA-PC-3 cells), when cultured in cell culture medium containing FBS with or without copper supplement. (B) Proliferation of DU-145 cells with knockdown of hCtr1 (Lenti-hCtr1-shRNA-DU145 cells) was slower than proliferation of DU-145 cells without knockdown of hCtr1 (Lenti-SCR-shRNA-DU145 cells), when cultured in cell culture medium containing FBS with or without copper supplement. Error bar, SD.

FIGURE 6. Quantification of tumor ^{64}Cu uptake by PET/CT of tumor-bearing mice injected with $^{64}CuCl_2$ as tracer. (A) ^{64}Cu radioactivity of PC-3 tumors with knockdown of hCtr1 (Lenti-hCtr1-shRNA-PC-3 tumor) was significantly lower than that of PC-3 tumors without knockdown of hCtr1 (Lenit-SCR-shRNA-PC-3 tumor). (B) ^{64}Cu radioactivity of DU-145 tumors with knockdown of hCtr1 (Lenti-hCtr1-shRNA-DU-145 tumor) was significantly lower than that of DU-145 tumor without knockdown of hCtr1 (Lenti-SCR-shRNA-DU-145 tumor). Error bar, SD.

cells for Lenti-hCtr1-shRNA-DU-145 cells) and the cells without knockdown of hCtr1 (686% $\pm$ 49% of inoculated cells for Lenti-SCR-shRNA-PC-3 cells, $P = 0.01$, and 981% $\pm$ 70% of inoculated cells for Lenti-SCR-shRNA-DU-145 cells, $P = 0.03$). When cultured in cell culture medium containing FBS supplemented with 10 μM $CuCl_2$ after serum starvation, the proliferation of Lenti-SCR-shRNA-PC-3 cells (883% $\pm$ 33% of inoculated cells) or Lenti-SCR-shRNA-DU-145 cells (1,393% $\pm$ 70% of inoculated cells) was significantly enhanced ($P < 0.01$), compared with proliferation of Lenti-SCR-shRNA-PC-3 cells (686% $\pm$ 49%) and Lenti-SCR-shRNA-DU-145 cells (981% $\pm$ 70%) cultured in cell culture medium containing FBS without copper supplement. However, the proliferation of Lenti-hCtr1-shRNA-PC-3 cells (495% $\pm$ 24% of inoculated cells) or Lenti-hCtr1-shRNA-DU-145 cells (930% $\pm$ 118% of inoculated cells) was not changed when cultured in cell culture medium containing FBS supplemented with 10 μM $CuCl_2$,
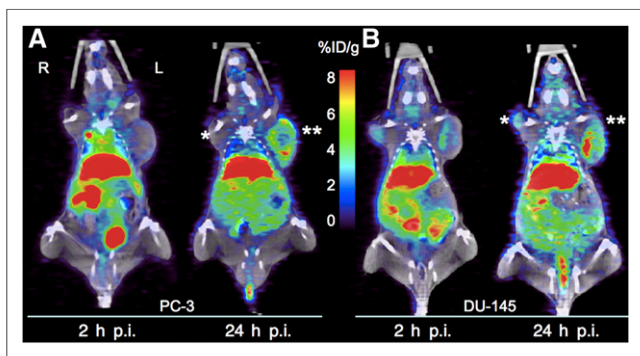

FIGURE 5. PET/CT of tumor-bearing mice injected with $^{64}CuCl_2$ as tracer. (A) Reduced ^{64}Cu radioactivity and growth inhibition of PC-3 tumor with knockdown of hCtr1 (Lenti-hCtr1-shRNA-PC-3 tumor on right, marked by *), compared with PC-3 tumors without knockdown of hCtr1 (Lenti-SCR-shRNA-PC-3 on left marked by **). (B) Reduced ^{64}Cu radioactivity and growth inhibition of DU-145 tumor with knockdown of hCtr1 (Lenti-hCtr1-shRNA-DU-145 tumor on right marked by *), compared with DU-145 tumors without knockdown of hCtr1 (Lenti-SCR-shRNA-DU-145 tumor on left marked by **). p.i. = postintravenous injection.
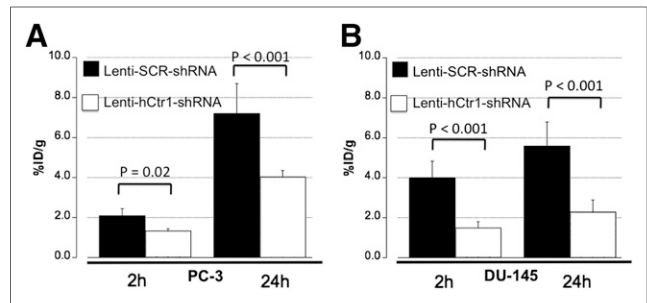
compared with proliferation of these cells cultured in cell culture medium containing FBS without copper supplement (458% $\pm$ 64% of inoculated cells for Lenti-hCtr1-shRNA-PC-3 cells and 804% $\pm$ 39% of inoculated cells for Lenti-hCtr1-shRNA-DU-145 cells), indicating hCtr1 is critical for copper-stimulated proliferation of prostate cancer cells.

Reduced Tumor ^{64}Cu Uptake and Growth Inhibition by Knockdown of hCtr1

Using PET/CT imaging, we determined a significant reduction of ^{64}Cu uptake in both PC-3 and DU-145 tumors with knockdown of hCtr1 (Lenti-hCtr1-shRNA-PC-3 tumors and Lenti-hCtr1-shRNA-DU145 tumors), as compared with ^{64}Cu uptake by the tumors without knockdown of hCtr1 (Lenti-SCR-shRNA-PC-3 tumors or Lenti-SCR-shRNA-DU-145 tumors; Figs. 5 and 6). At 2 h after injection, the ^{64}Cu radioactivity of the Lenti-hCtr1-shRNA-PC-3 tumors was determined as (1.35 $\pm$ 0.08 %ID/g) by PET quantification, which was significantly lower than the ^{64}Cu radioactivity of the control Lenti-SCR-shRNA-PC-3 tumors (2.10 $\pm$ 0.36 %ID/g, $P = 0.02$). Moreover, the ^{64}Cu radioactivity of the Lenti-hCtr1-shRNA-DU-145 tumors was determined as 1.51 $\pm$ 0.30 %ID/g, which was also significantly lower than the ^{64}Cu radioactivity of the control Lenti-SCR-shRNA-DU-145 tumors (4.03 $\pm$ 0.80 %ID/g, $P < 0.001$). The decrease in ^{64}Cu uptake was even more obvious in PET images obtained at 24 h after injection. At 24 h after injection, the ^{64}Cu radioactivity of the Lenti-hCtr1-shRNA-PC-3 tumors (4.02 $\pm$ 0.31 %ID/g) was significantly lower than that of the control Lenti-SCR-shRNA-PC-3 tumors (7.21 $\pm$ 1.48 %ID/g, $P < 0.001$), as was the case in DU-145 tumors (2.30 $\pm$ 0.59 %ID/g in Lenti-hCtr1-shRNA-DU-145 tumors vs. 5.57 $\pm$ 1.20 %ID/g in control Lenti-SCR-shRNA-DU-145 tumors; $P < 0.001$). The findings of PET quantitative analysis were confirmed by tumor ^{64}Cu radioactivity from postmortem tissue radioactivity assay (Table 1). Knockdown of hCtr1 was associated with tumor growth inhibition as visualized on PET/CT (Fig. 5) and ex vivo tumor size measurement (Fig. 7A). The tumor volume of Lenti-hCtr1-shRNA PC-3 tumors (179 $\pm$ 111 mm³) was found to be significantly smaller than that of Lenti-SCR-shRNA PC-3 tumors (536 $\pm$ 191 mm³, $P < 0.01$) at 4 wks after implantation of the cells (Fig. 7B). Similarly, tumor volume of Lenti-hCtr1-shRNA-DU-145 tumors (39 $\pm$ 22 mm³) was found to be significantly smaller than that of Lenti-SCR-shRNA DU-145 tumors (208 $\pm$ 104 mm³, $P < 0.01$) at 7 wks after implantation of the cells (Fig. 7B).

[Fig. 5]
[Fig. 6]
[Table 1]
[Fig. 7]

Tissue	Tissue ^{64}Cu radioactivity from mice with PC-3 prostate cancer xenografts (%ID/g)	Tissue ^{64}Cu radioactivity from mice with DU-145 prostate cancer xenografts (%ID/g)
Liver	22.7 ± 14.2	20.1 ± 8.8
Spleen	3.9 ± 1.4	5.0 ± 5.7
Kidney	12.4 ± 6.1	5.3 ± 3.0
Heart	7.2 ± 4.9	2.7 ± 0.9
Muscle	1.0 ± 0.6	0.4 ± 0.3
Brain	0.9 ± 0.7	0.3 ± 0.1
Blood	2.0 ± 1.0	1.5 ± 0.5
Testis	1.3 ± 0.4	0.9 ± 0.5
Tumors without knockdown of hCtr1	6.6 ± 1.1 (Lenti-SCR-shRNA-PC-3)	5.7 ± 5.3 (Lenti-SCR-shRNA-DU-145)
Tumors with knockdown of hCtr1	3.6 ± 0.7 (Lenti-hCtr1-shRNA-PC-3)	2.8 ± 2.0 (Lenti-hCtr1-shRNA-DU-145)

DISCUSSION

Copper is required for cell proliferation, but excess copper is paradoxically cytotoxic. Copper homeostasis is tightly regulated by a delicate network of influx copper transporter (hCtr1), efflux copper transporters (ATP7A and ATP7B), copper chaperons (ATOX1, Cox17, CCS), and other copper binding molecules (26). In this study, we prepared polyclonal antibody specific for hCtr1 using recombinant hCtr1 protein expressed in *Escherichia coli* because the polyclonal hCtr1 antibody used previously (16) was not suitable for Western blot. Using newly prepared polyclonal antibody, we demonstrated elevated expression of hCtr1 in prostate cancer cells (PC-3, DU145, and C4-2) and immortalized prostate epithelial cells containing HPV oncogene (PZ-HPV-7, RWPE-1, RWPE-2) by Western blot, compared with hCtr1 expression in normal prostate epithelial cells (Fig. 1B). Previous detection of a low level of hCtr1 mRNA in PZ-HPV-7 cells by qRT-PCR in a prior study (27) might be due to variation of hCtr1 expression in the PZ-HPV-7 cells or a stability issue of the RNA samples used

RGB

FIGURE 7. Suppression of tumor growth by knockdown of hCtr1 in human prostate cancer xenografts in mice. (A) Tumors with knockdown of hCtr1 (Lenti-hCtr1-shRNA-PC-3 tumor and Lenti-hCtr1-shRNA-DU-145 tumor) were smaller than those without knockdown of hCtr1 (Lenti-SCR-shRNA-PC-3 tumor and Lenti-SCR-shRNA-DU-145 tumor), at 4 wks after implantation of PC-3 cells and 7 wks after implantation of DU-145 cells, respectively. (B) Volumes of tumors with knockdown of hCtr1 (Lenti-hCtr1-shRNA-PC-3 and Lenti-hCtr1-shRNA-DU-45) were significantly smaller than those without knockdown of hCtr1 (Lenti-SCR-shRNA-PC-3 and Lenti-SCR-shRNA-DU-145), based on calculation from tumor size measured ex vivo with caliper. Error bar, SD.

for that study. The reduction of cellular and tumor ^{64}Cu uptake by RNAi-mediated knockdown of hCtr1 (Figs. 3 and 5) indicated that hCtr1 plays an important role in mediating the copper uptake required for uncontrolled proliferation of prostate cancer cells. Although hCtr1 expression in DU-145 cells was slightly higher than hCtr1 expression in PC-3 cells (Fig. 1), ^{64}Cu uptake by tumors derived from DU-145 prostate cancer cells was found to be lower than ^{64}Cu uptake by tumors derived from PC-3 cells (Figs. 3, 5, and 6). This difference might be related to variable expression of copper transporters, chaperons, or other copper carrier molecules, for example, metheothinine (28), between these 2 prostate cancer cells lines. Tumor uptake of ^{64}Cu is expected to be variable based on the profile of various copper transporters, chaperons, and copper binding molecules, not simply depending on the expression level of hCtr1, supported by the findings from other investigators (29). Additional studies of the expression of hCtr1 and other copper transporters in the tumor tissue samples from the patients are warranted to determine their role in copper metabolism of prostate cancer. There has been increased interest in development of ^{64}Cu radiopharmaceuticals for cancer imaging and therapy (30–32). Given expected variation of tumor ^{64}Cu uptake, it is essential to set up appropriate controls to differentiate tumor uptake of free ^{64}Cu ions disassociated from ^{64}Cu-radiolabeled conjugates from tumor uptake of intact ^{64}Cu-radiolabeled conjugates in the characterization of ^{64}Cu-radiolabeled radiopharmaceuticals.

Prostate cancer is a heterogeneous disease characterized by variable genomic alterations, including different point mutations and chromosomal alterations such as deletions, insertions, or translocations (1,2). Given the complex heterogeneity of prostate cancer, the metabolism of prostate cancer may vary among different patients, even among different tumor lesions in the same individual patient diagnosed with prostate cancer. It is not surprising to have variable uptake of radiopharmaceuticals used for metabolic imaging of prostate cancer, including variable uptake of radiotracer ^{11}C choline in prostate cancer (33). It is expected that copper metabolism of prostate cancer may vary in different patients, even in different lesions of prostate cancer in the same patient. Although it remains to be determined whether the use of $^{64}CuCl_2$ PET/CT for screening or early diagnostic imaging of primary prostate cancer will be limited by the variability of copper metabolism, $^{64}CuCl_2$ PET/CT might be useful for assessing copper metabolism of prostate cancer lesions detected by PET using a probe targeting a biomarker present on most prostate cancer cells, such as a radiopharmaceutical agent
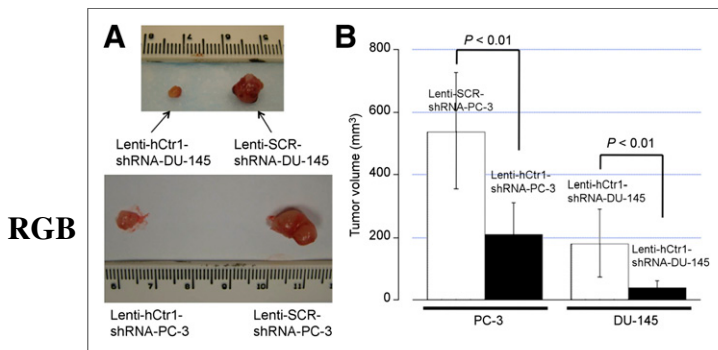
targeting prostate-specific membrane antigen (*34*), humanized radioiodinated minibody targeting prostate stem cell antigen (*35*), and radiolabeled peptide agent targeting vasoactive intestinal polypeptide receptor 1 (*36*). On the basis of requirement of copper for cell proliferation and tumor angiogenesis, and the recent finding that copper promotes invasion of the prostate cancer epithelial cells (*37*), it is postulated that copper metabolism status may be related to aggressiveness and metastasis of prostate cancer. Copper metabolism holds potential as a prognostic imaging biomarker in prostate cancer, using ^{64}CuCl$_2$ PET/CT. Safe usage of ^{64}CuCl$_2$ for the PET/CT imaging of human prostate cancer is supported by the prior use of ^{64}CuCl$_2$ for the assessment of copper metabolism in healthy human subjects and copper metabolism disorders in patients diagnosed with Wilson's disease without significant side effects (*38,39*); tiny amount of copper ions in a tracer dose of ^{64}CuCl$_2$ and reduction of Cu(II) ions for cellular uptake of Cu(I) ions mediated by hCtr1 (*26*), which should ease the concern of cytotoxicity of Cu(II) ions from ^{64}CuCl$_2$; and data from the recent radiation dosimetry of ^{64}CuCl$_2$ in a *ATP7b$^{-/-}$* knockout mouse model of Wilson's disease, suggesting the safe usage of ^{64}CuCl$_2$ as a radioactive tracer for PET imaging in humans (*24*).

RNAi-mediated knockdown of hCtr1 was associated with the suppression of prostate cancer cell proliferation in vitro (Fig. 4). The molecular mechanism of suppression of cell proliferation by knockdown of hCtr1 remains to be illustrated, which may be related to a functional loss of some copper-requiring molecules regulating cell proliferation or abolishment of cell growth–stimulating activity of hCtr1 itself or disruption of its interaction with other molecules regulating cell proliferation. Knockdown of hCtr1 was associated with growth inhibition of prostate cancer xenografts in vivo (Fig. 7). We noted that growth of prostate cancer xenograft tumors derived from DU-145 cells was slower than growth of tumors derived from PC-3 prostate cancer cells (Fig. 7), although the level of hCtr1 expression in DU-145 cells was higher than the level of hCtr1 expression in PC-3 cells by Western blot (Fig. 1B). Differences in the growth of tumors derived from PC-3 and DU-145 cells may be related to the effects of other growth factors that are differentially expressed in PC-3 cells and enhance growth of tumors derived from PC-3 prostate cancers in vivo. The molecular mechanism of tumor growth inhibition by knockdown of hCtr1 remains to be elucidated, which may be related to reduction of cancer cell proliferation and suppression of tumor angiogenesis. It will be intriguing to study the effect of hCtr1 knockdown on cancer cell proliferation in vivo by PET/CT of tumor-bearing mice using 3′-deoxy-3′-^{18}F-fluorothymidine (*40*), in conjunction with study of other molecules regulating cell proliferation.

CONCLUSION

Reduced tumor ^{64}Cu uptake and tumor growth inhibition by RNAi-mediated knockdown of hCtr1 suggest that hCtr1 is a promising new theranostic target, which can be further developed for metabolic imaging of prostate cancer using ^{64}CuCl$_2$ PET/CT and personalized cancer therapy targeting copper metabolism.

DISCLOSURE

ACKNOWLEDGMENTS

REFERENCES

1. Berger MF, Lawrence MS, Demichelis F, et al. The genomic complexity of primary human prostate cancer. *Nature*. 2011;470:214–220.
2. Boyd LK, Mao XY, Lu YJ. The complexity of prostate cancer: genomic alterations and heterogeneity. *Nat Rev Urol*. 2012;9:652–664.
3. Schöder H, Larson SM. Positron emission tomography for prostate, bladder, and renal cancer. *Semin Nucl Med*. 2004;34:274–292.
4. Som P, Atkins HL, Bandoypadhyay D, et al. A fluorinated glucose analog, 2-fluoro-2-deoxy-D-glucose [^{18}F]: nontoxic tracer for rapid tumor detection. *J Nucl Med*. 1980;21:670–675.
5. Hara T, Kosaka N, Kishi H. PET imaging of prostate cancer using carbon-11-choline. *J Nucl Med*. 1998;39:990–995.
6. DeGrado TR, Coleman RE, Wang S, et al. Synthesis and evaluation of ^{18}F-labeled choline as an oncologic tracer for positron emission tomography: initial findings in prostate cancer. *Cancer Res*. 2001;61:110–117.
7. Hara T, Kosaka N, Kishi H. Development of ^{18}F-fluoroethylcholine for cancer imaging with PET: synthesis, biochemistry, and prostate cancer imaging. *J Nucl Med*. 2002;43:187–199.
8. Oyama N, Akino H, Kanamaru H, et al. ^{11}C-acetate PET imaging of prostate cancer. *J Nucl Med*. 2002;43:181–186.
9. Sun H, Sloan A, Mangner TJ, et al. Imaging DNA synthesis with [^{18}F]FMAU and positron emission tomography in patients with cancer. *Eur J Nucl Med Mol Imaging*. 2005;32:15–22.
10. Tóth G, Lengyel Z, Balkay L, et al. Detection of prostate cancer with ^{11}C-methionine positron emission tomography. *J Urol*. 2005;173:66–69.
11. Theophanides T, Anastassopoulou J. Copper and carcinogenesis. *Crit Rev Oncol Hematol*. 2002;42:57–64.
12. Nasulewicz A, Mazurb A, Opolski A. Role of copper in tumour angiogenesis: clinical implications. *J Trace Elem Med Biol*. 2004;18:1–8.
13. Turski ML, Thiele DJ. New roles for copper metabolism in cell proliferation, signaling, and disease. *J Biol Chem*. 2009;284:717–721.
14. Wiederanders RE, Evans GW. The copper concentration of hyperplastic and cancerous prostates. *Invest Urol*. 1969;6:531–533.
15. Margalioth EJ, Schenker JG, Chevion M. Copper and zinc levels in normal and malignant tissues. *Cancer*. 1983;52:868–872.
16. Peng F, Lu X, Janisse J, Muzik O, Shields AF. Positron emission tomography of human prostate cancer xenografts in mice with increased uptake of copper (II)-64 chloride. *J Nucl Med*. 2006;47:1649–1652.
17. Zhou B, Gitschier J. hCTR1: a human gene for copper uptake identified by complementation in yeast. *Proc Natl Acad Sci USA*. 1997;94:7481–7486.
18. Brummelkamp TR, Bernards R, Agami R. A system for stable expression of short interfering RNAs in mammalian cells. *Science*. 2002;296:550–553.
19. Aller SG, Unger VM. Projection structure of the human copper transporter CTR1 at 6-Å resolution reveals a compact trimer with a novel channel-like architecture. *Proc Natl Acad Sci USA*. 2006;103:3627–3632.
20. Klomp AE, Tops BB, Van DenBerg IE, Erger R, Klomp LW. Biochemical characterization and subcellular localization of human copper transporter 1 (hCTR1). *Biochem J*. 2002;364:497–505.
21. Xie D, Gore C, Liu J, et al. Role of DAB2IP in modulating epithelial-to-mesenchymal transition and prostate cancer metastasis. *Proc Natl Acad Sci USA*. 2010;107:2485–2490.
22. Cai H, Peng F. Knockdown of copper chaperon antioxidant-1 by RNA interference inhibited copper-stimulated proliferation of non-small cell lung carcinoma cells. *Oncol Rep*. 2013;30:269–275.
23. Ishiyama M, Miyazono Y, Sasamoto K, Ohkura Y, Ueno K. A highly water-soluble disulfonated tetrazolium salt as a chromogenic indicator for NADH as well as cell viability. *Talanta*. 1997;44:1299–1305.

24. Peng F, Lutsenko S, Sun X, Muzik O. Positron emission tomography of copper metabolism in the Atp7b −/− knock-out mouse model of Wilson's disease. *Mol Imaging Biol.* 2012;14:70–78.

25. Tomayko MM, Reynolds CP. Determination of subcutaneous tumor size in athymic (nude) mice. *Cancer Chemother Pharmacol.* 1989;24:148–154.

26. Lutsenko S. Human copper homeostasis: a network of interconnected pathways. *Curr Opin Chem Biol.* 2010;14:211–217.

27. Zhang H, Cai H, Lu X, Muzik O, Peng F. Positron emission tomography of human hepatocellular carcinoma xenografts in mice using copper (II)-64 chloride as a tracer. *Acad Radiol.* 2011;18:1561–1568.

28. Yu M, Huai Q, Huang G, et al. Biodistribution of [^{64}Cu]Cu2 + and variance of metallothionein during tumor treatment by copper. *Nucl Med Biol.* 1998;25:111–116.

29. Jørgensen JT, Persson M, Madsen J, Kjær A. High tumor uptake of ^{64}Cu: implications for molecular imaging of tumor characteristics with copper-based PET tracers. *Nucl Med Biol.* 2013;40:345–350.

30. Lewis MR, Wang M, Axworthy DB, et al. In vivo evaluation of pretargeted ^{64}Cu for tumor imaging and therapy. *J Nucl Med.* 2003;44:1284–1292.

31. Hao G, Singh AN, Oz OK, Sun X. Recent advances in copper radiopharmaceuticals. *Curr Radiopharm.* 2011;4:109–121.

32. Wang H, Chen X. Visualization of copper metabolism by ^{64}CuCl$_2$-PET. *Mol Imaging Biol.* 2012;14:14–16.

33. Nanni C, Schiavina R, Boschi S, et al. Comparison of ^{18}F-FACBC and ^{11}C-choline PET/CT in patients with radically treated prostate cancer and biochemical relapse: preliminary results. *Eur J Nucl Med Mol Imaging.* 2013;40(suppl 1): S11–S17.

34. Chen Y, Foss CA, Byun Y, et al. Radiohalogenated prostate-specific membrane antigen (PSMA)-based ureas as imaging agents for prostate cancer. *J Med Chem.* 2008;51:7933–7943.

35. Leyton JV, Olafsen T, Lepin EJ, et al. Humanized radioiodinated minibody for imaging of prostate stem cell antigen-expressing tumors. *Clin Cancer Res.* 2008;14:7488–7496.

36. Zhang K, Aruva MR, Shanthly N, et al. PET imaging of VPAC1 expression in experimental and spontaneous prostate cancer. *J Nucl Med.* 2008;49:112–121.

37. Parr-Sturgess CA, Tinker CL, Hart CA, Brown MD, Clarke NW, Parkin ET. Copper modulates zinc metalloproteinase-dependent ectodomain shedding of key signaling and adhesion proteins and promotes the invasion of prostate cancer epithelial cells. *Mol Cancer Res.* 2012;10:1282–1293.

38. Bush JA, Mahoney JP, Markowitz H, Gubler CJ, Cartwright GE, Wintrobe MM. Studies on copper metabolism. XVI. Radioactive copper studies in normal subjects and in patients with hepatolenticular degeneration. *J Clin Invest.* 1955;34: 1766–1778.

39. Walshe JM, Potter G. The pattern of the whole body distribution of radioactive copper (^{67}Cu, ^{64}Cu) in Wilson's disease and various control groups. *Q J Med.* 1977;46:445–462.

40. Shields AF, Grierson JR, Dohmen BM, et al. Imaging proliferation in vivo with [F-18]FLT and positron emission tomography. *Nat Med.* 1998;4:1334–1336.